AIAA JOURNAL
Vol. 39, No. 7, July 2001

Effects of Forward Flight on Jet Mixing Noise from Fine-Scale Turbulence

Christopher K. W. Tam,* Nikolai Pastouchenko,† and Laurent Auriault†
Florida State University, Tallahassee, Florida 32306-4510

It is known experimentally that a jet in forward flight radiates less noise than the same jet in a static environment. At a forward flight Mach number of 0.2, the noise reduction, depending on the jet operating conditions, could be as large as 4–5 dB in the sideline directions. In the past, a way to predict flight effects was to use the method of relative velocity exponent. Another method was to extrapolate measured static jet noise to the flight condition by means of scaling formulas. Both methods are semi-empirical. The fine scale turbulence jet mixing noise theory of Tam and Auriault (Tam, C. K. W., and Auriault, L., "Jet Mixing Noise from Fine Scale Turbulence," *AIAA Journal*, Vol. 37, No. 2, 1999, pp. 145–153) is extended for application to jets in simulated forward flight. It will be shown that the calculated noise spectra at different simulated forward flight Mach numbers for both supersonic and subsonic jets compare well with experiments. The effects of forward flight on the sources of fine-scale turbulent jet mixing noise is also investigated. It is found that in the presence of forward flight the dominant noise sources move downstream. The turbulence intensity and the size of turbulent eddies responsible for noise emission are reduced.

I. Introduction

EXPERIMENTALLY, it has been found that a jet in forward flight emits less noise than the same jet in a static environment. The decrease in noise intensity is quite substantial. For instance, at forward flight Mach number 0.2, there is a drop of 4–5 dB in the noise radiated to the sideline.

The standard practice to quantify the effect of forward flight on jet noise in a laboratory is to put the jet inside an open wind tunnel and measure the emitted noise by microphones mounted outside. In this arrangement, the flow around the jet will be the same as that in actual forward flight when viewed from the nozzle-fixed coordinate. In the literature, such data are referred to as simulated forward flight measurements.[1–4] During the 1970s and early 1980s, two methods were established for predicting the effects of forward flight on the noise of high-speed jets. Both were semi-empirical methods. One method used was the so-called relative velocity exponent[5,6] whereby the noise intensity was taken to be proportional to a high power of the relative velocity between the jet and the outside flow. The velocity exponent was found empirically. The other was a scaling method.[7,8] In this case, the measured noise of a static jet was extrapolated to the forward flight condition by semi-empirical formulas.

Beginning in the early 1990s, high-quality narrowband jet noise data became available. At the same time, there was a much better understanding of the nature and characteristics of jet turbulence. These, together with the development of high-quality turbulence models and computational aeroacoustics methods, made it possible for the development of significantly improved understanding of the sources of jet mixing noise. Subsequently, an accurate noise prediction theory was established.

Tam et al.[9] (see also Ref. 10) found, after examining the entire data bank of the Jet Noise Laboratory of the NASA Langley Research Center, that the spectrum of turbulent mixing noise from high-speed jets appeared to fit two seemingly universal spectra (for convenience of reference, these spectra will be referred to as the TGS-1 and TGS-2 spectra) regardless of jet Mach number and temperature ratio. This unexpected finding indicates that jet mixing noise consists of two main components. To provide a physical meaning to the two spectra, Tam et al.[9] noted that during the past 25 years there were overwhelming evidence that jet turbulence comprised both large and small scales. For high-speed jets, optical observations and theoretical analysis[11,12] indicated that the large turbulence structures of the jet flow, behaving like traveling wavy walls, emitted intense Mach wave radiation in the downstream direction. In the downstream direction, all of the noise spectra were observed to fit the TGS-1 spectrum well. Based on this, it was proposed that the TGS-1 spectrum was a distinctive characteristic of large turbulence structures noise. Tam et al.[9] also recognized that the fine-scale turbulence was more isotropic and would, therefore, emit noise without a strong directivity. Because there was little large turbulence structures noise in the sideline and upstream directions, the noise in these directions must be that from the fine-scale turbulence. In the sideline and upstream directions, the noise was found to fit the TGS-2 spectrum well. Thus it was proposed that this spectrum was a feature of fine-scale turbulence noise.

Since the identification of the TGS-1 and TGS-2 spectra, Tam[13] found that these same spectra shapes also fitted the measured noise of jets from rectangular, elliptic, and plug nozzles well. In a recent investigation, Dahl et al.[14] demonstrated that the two TGS spectra provided excellent fit to their coaxial jet noise data. Wat et al.,[15] on the other hand, performed analysis to a large set of flyover jet noise data. They reported that the data had the spectral shape of the TGS spectra. Most recently, Tam and Zaman[16] measured the noise from subsonic jets issued from circular, rectangular, elliptic, as well as lobe nozzles. Despite the large difference in nozzle shape, it was found that all of the measured noise spectra fit favorably the TGS spectra.

In this work, our interest is on the sideline noise. Thus, the present investigation will be confined only to the effects of forward flight on the fine-scale turbulence noise of jets. The present investigation is based on the recently developed fine-scale turbulence jet noise theory of Tam and Auriault.[17] Unlike many other jet noise theories, the Tam and Auriault theory is a self-contained prediction theory. The theory begins with the recognition, using the gas kinetic theory analogy, that the time fluctuations of the fine-scale turbulence kinetic energy is the main source of noise. The theory accounts for mean flow refraction, as well as the source convection effect. The turbulence information needed by the theory for noise prediction purpose is provided by the k–ε turbulence model. The theory contains three additional constants beyond those of the k–ε model. These three constants were determined by best fit to a large set of data. Tam and Auriault showed, by comparison with experimental measurements, that the theory could predict the fine-scale turbulence noise spectrum accurately over a large range of jet Mach number and jet to ambient temperature ratio.

Received 26 May 2000; presented as Paper 2000-2061 at the AIAA/CEAS 6th Aeroacoustics Conference, Lahaina, HI, 12–14 June 2000; revision received 20 December 2000; accepted for publication 26 December 2000.

*Robert O. Lawton Distinguished Professor, Department of Mathematics. Fellow AIAA.

†Graduate Student, Department of Mathematics.

One of the objectives of this work is to use the Tam and Auriault[17] theory, without any modifications of the constants, to predict the noise of high-speed jets in simulated forward flight. It will be shown that the calculated sideline noise spectra at different forward flight Mach numbers for both supersonic and subsonic jets agree well with experimental measurements. Because the theory as used involves no additional adjustable constant, the calculated jet noise spectra in simulated forward flight may be regarded as absolute predictions.

Another objective of this investigation is to study the effects of forward flight on the sources of fine-scale jet mixing noise. Of particular interest are the noise intensity and location. Information of this kind is useful for noise suppression purposes. Forward flight obviously would also affect the far-field noise through changes in the mean flow refraction. However, in this work, our primary concern is with source modification alone.

In Sec. II, the Tam and Auriault theory[17] is extended to the flow configuration of a high-speed jet in an open wind tunnel to determine the effects of forward flight on jet mixing noise. The first step of the theory involves the prediction of the jet mean flow and the basic turbulence quantities. Extensive comparisons between the calculated mean flow profiles and experimental measurements are provided. The second step of the theory is to predict the radiated sound. It will be shown that the theoretical noise spectra at different forward flight Mach numbers are in good agreement with experiments. Section III is devoted to an assessment of the effects of forward flight on the sources of fine-scale turbulence noise. The changes in noise source are the direct consequence of the effect of forward flight on the turbulence of the jet. Therefore, the changes in the turbulence intensity and other relevant turbulence quantities are also investigated.

II. Open Wind-Tunnel Simulation of Forward Flight

Forward flight effects on jet noise may be assessed by outdoor flyover measurements. However, such experiments are expensive and difficult to control. To provide a controllable and repeatable experimental environment, most forward flight experiments are done using an open wind tunnel inside an anechoic chamber. The jet is mounted in the potential core of the wind tunnel. Far-field microphones are placed outside the wind-tunnel flow. By measuring the jet noise with and without the wind-tunnel flow on, one can obtain quantitative changes in jet mixing noise due to forward flight. In the nozzle-fixed coordinate system, the flow around the jet in a simulated forward flight experiment is no different from that of the jet in actual flight. In terms of possible source modification by the ambient flow, the flow physics is completely reproduced in a simulated forward flight experiment. Because of the presence of an outer shear layer surrounding the open wind tunnel, the mean flow refraction effect, however, is not the same. This difference should be borne in mind when interpreting the measured or computed data.

In this work, we will apply the Tam and Auriault[17] jet mixing noise theory to the open wind-tunnel simulated forward flight flow configuration. Before we present the computed results it seems useful to first describe the theory briefly. Tam and Auriault examined how the kinetic energy of the random velocity fluctuations of a gas contributed to the pressure of the gas in kinetic theory of gasses. They reasoned that in a turbulent flow, by analogy, pressure fluctuations can be generated by the time fluctuations of the turbulent kinetic energy of the fine-scale turbulence. The pressure fluctuations would give rise to compression and rarefaction in the fluid medium. This results in acoustic disturbances. Thus, the fluctuation of turbulence kinetic energy is the source of turbulent mixing noise in a jet. In nearly equilibrium flows, such as jets, the fluctuating part of the turbulence kinetic energy would scale with the time-independent part. This then allows one to use the k–ε turbulence model to provide the necessary turbulence information, for example, intensity, length, and timescales needed for noise prediction.

In the Tam and Auriault[17] theory, a number of steps have to be carried out before the radiated noise can be calculated. Without getting into great detail, it is sufficient to say that the first major task is to calculate the mean flow and the turbulence quantities through the k–ε turbulence model. The second task is to determine the mean flow refraction effect using the mean flow found in step one. In Tam and Auriault's work, this is done by the use of the adjoint Green's function following the method of Ref. 18. The third task is to determine the radiated noise spectrum by the use of a model two-point space–time correlation function of the time fluctuation of the kinetic energy of the fine-scale turbulence. In this way, the following formulas for the far-field noise spectrum, $S(R, \Theta, \phi, fD_j/u_j)$, in decibel per Strouhal number (fD_j/u_j) are derived:

$$S\left(R, \Theta, \phi; \frac{fD_j}{u_j}\right) = 10\log\left[\frac{S(R, \Theta, \phi, f)}{p_{\text{ref}}^2(D_j/u_j)}\right] \tag{1}$$

where

$$S(R, \Theta, \phi, f) = 4\pi \tilde{S}(R, \Theta, \phi, \omega)$$

$$\tilde{S}(R, \Theta, \phi, \omega) = 4\pi\left(\frac{\pi}{\ell n 2}\right)^{\frac{3}{2}} \iiint_{\text{jet}} \frac{\hat{q}_S^2 \ell_S^3}{c^2 \tau_S} \times \left\{\frac{|p_a(\boldsymbol{x}_2, \boldsymbol{x}, \omega)|^2 \exp\left[-\omega^2 \ell_S^2 \big/ \bar{u}^2 (4\,\ell n 2)\right]}{\left\{1 + \omega^2 \tau_S^2 [1 - (\bar{u}/a_\infty)\cos\Theta]^2\right\}}\right\} \mathrm{d}\boldsymbol{x}_2 \tag{2}$$

Equations (1) and (2) are Eqs. (35) and (36) of Ref. 17. Here $\boldsymbol{x}_2$ is the source point, and $\boldsymbol{x}$ is the far-field measurement point with spherical coordinates (R, Θ, ϕ). The spherical coordinate system is centered at the nozzle exit with the polar axis in the direction of flow. Θ is the polar angle, and ϕ is the azimuthal angle. Also $\omega = 2\pi f$ is the angular frequency, and p_{ref} is the reference pressure for the decibel scale. D_j and u_j are the fully expanded jet diameter and velocity, respectively, and fD_j/u_j (denoted by Sr) is the Strouhal number. Equation (2) contains a number of turbulence quantities including $\hat{q}_S$, the fine-scale turbulence intensity; ℓ_S, the eddy size; and τ_S, the eddy decay time. They are related to k, the turbulence kinetic energy, and ε, the dissipation rate, of the k–ε turbulence model as follows:

$$\ell_S = c_\ell \ell = c_\ell\left(k^{\frac{3}{2}} \big/ \varepsilon\right), \qquad \tau_S = c_\tau \tau = c_\tau (k/\varepsilon) \tag{3}$$

$$\hat{q}_S^2 \big/ c^2 = A^2 q^2, \qquad q = \tfrac{2}{3}\bar{\rho} k \tag{4}$$

where $\bar{\rho}$ is the density of the jet mean flow at $\boldsymbol{x}_2$ and c_ℓ, c_τ, and A are the three empirical constants of the theory. Their numerical values, as determined by the best fit to the data,[17] are

$$c_\ell = 0.256, \qquad c_\tau = 0.233, \qquad A = 0.755 \tag{5}$$

In addition, $\bar{u}$ is the mean flow velocity at $\boldsymbol{x}_2$ and a_∞ is the ambient speed of sound. Here $p_a(\boldsymbol{x}_2, \boldsymbol{x}, \omega)$ is the adjoint pressure Green's function (see Ref. 18).

Note that one advantage of using the adjoint Green's function method to calculate the noise of jets in simulated forward flight is that the refraction effect of the outer shear layer of the open wind tunnel is automatically included in the computation. No (traditional) shear layer correction is needed.

A. Jet Exit Conditions

In the work of Tam and Auriault,[17] the mean flow of the jet as well as the values of k and ε are calculated by a parabolized spatial marching algorithm developed by Thies and Tam.[19] The marching algorithm uses the dispersion-relation-preserving scheme[20] and starts the computation at the nozzle exit plane. To initialize the computation, the velocity and temperature profiles at the nozzle exit plane must be given. In all of the present computations, we use the velocity and temperature profiles of Figs. 1 and 2 as initial condition. Figure 1 shows the radial profile of the jet exit velocity. In Fig. 1, r is the radial coordinate of a cylindrical coordinate system centered at the nozzle exit. The jet velocity is u_j, the open wind-tunnel velocity is u_f, and the radius of the uniform core region of the jet is r_j. The uniform core region of the open wind tunnel extends from $r = r_3$ to r_4. Between the two core regions is the wake region formed just downstream of the nozzle lip. The minimum velocity is u_e, which

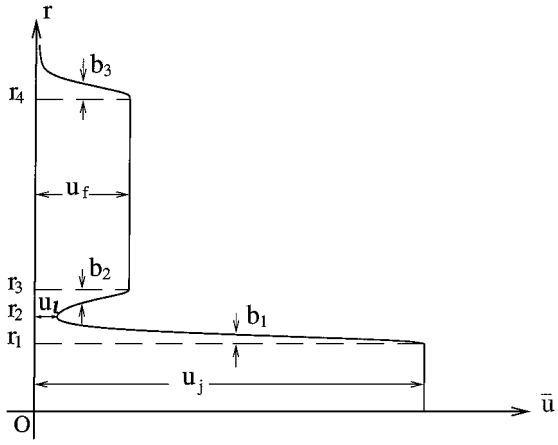

Fig. 1 Radial profile of jet velocity at the nozzle exit plane.

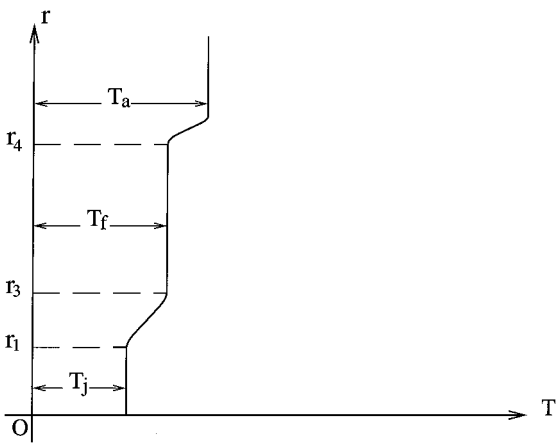

Fig. 2 Radial profile of jet temperature at the nozzle exit plane.

may be equal to zero, at r_2. Analytically, the mean flow profile $\bar{u}(r)$ is assumed to have the form

$$\bar{u} = \begin{cases} u_j, & r \le r_1 \\ u_1 + (u_j - u_1)\exp\left\{-(\ell n 2)[(r - r_1)/b_1]^2\right\}, & r_1 \le r \le r_2 \\ u_2 + (u_f - u_2)\exp\left\{-(\ell n 2)[(r - r_3)/b_2]^2\right\}, & r_2 \le r \le r_3 \\ u_f, & r_3 \le r \le r_4 \\ u_f \exp\left\{-(\ell n 2)[(r - r_4)/b_3]^2\right\}, & r_4 \le r \end{cases} \tag{6}$$

where

$$u_1 = \frac{u_e - u_j \exp\left\{-(\ell n 2)[(r_2 - r_1)/b_1]^2\right\}}{1 - \exp\left\{-(\ell n 2)[(r_2 - r_1)/b_1]^2\right\}}$$

$$u_2 = \frac{u_e - u_f \exp\left\{-(\ell n 2)[(r_2 - r_3)/b_2]^2\right\}}{1 - \exp\left\{-(\ell n 2)[(r_2 - r_3)/b_2]^2\right\}}$$

Velocity profile (6) is characterized by the parameters r_1, r_2, r_3, r_4, b_1, b_2, b_3, and u_e, in addition to u_j and u_f. In cases where a measured velocity profile near the nozzle exit is available, these parameters are adjusted to give the best fit to the data at this station. The computation will continue downstream without further adjustment. If no velocity profile is available, the best estimated values of the parameters are used in the computation.

Figure 2 is the radial profile of jet temperature at the nozzle exit plane. T_j, T_f, and T_a are the jet, the wind tunnel, and the ambient temperature, respectively. The analytical form of the temperature profile used in the computation is

$$T = \begin{cases} T_j, & r \le r_1 \\ T_1 + (T_f - T_1)\exp\left\{-(\ell n 2)[(r_3 - r)/b_1]^2\right\}, & r_1 \le r \le r_3 \\ T_f, & r_3 \le r \le r_4 \\ T_a + (T_f - T_a)\exp\left\{-(\ell n 2)[(r - r_4)/b_2]^2\right\}, & r > r_4 \end{cases} \tag{7}$$

where

$$T_1 = \frac{T_j - T_f \exp\left\{-(\ell n 2)[(r_3 - r_1)/b_1]^2\right\}}{1 - \exp\{-(\ell n 2)[(r_3 - r_1)/b_1]^2\}}$$

In all of the computations in this paper, the starting values for k and ε are taken to be 10^{-6} and 10^{-4}, respectively.

B. Comparison Between Calculated Mean Flow Profiles and Experiment

As stated before, the first step in implementing the Tam and Auriault[17] theory is to calculate the jet mean flow as well as the distributed values of k and ε throughout the jet. This is carried out using the algorithm and computer code of Thies and Tam.[19] The initial conditions of Eqs. (6) and (7) are used at the nozzle exit plane. In this section, we wish to present detailed comparisons between the calculated velocity profiles and experimental measurements. For this purpose, the parameters of Eqs. (6) and (7) are chosen so that the computed profile matches that of the experiment at the first measurement station closest to the nozzle exit.

Figure 3 compares the computed and measured centerline velocity distribution of a Mach 0.47 cold jet at 10% and 20% forward velocity ratio (u_f/u_j). The data are from Ref. 21. Figures 4a and 4b show the corresponding radial profiles of jet velocity at four locations downstream.

Figure 5 shows the measured and the computed centerline velocity distributions of two high-speed jets. One is a coaxial jet from Ref. 22. The inner jet is hot, operating at 657 K. The jet exit velocity is 411 m/s. The outer jet is cold at 292 K and has a velocity of 274 m/s. The other jet is a cold Mach 0.9 jet at 10% forward flight speed from Ref. 21. Figure 6a shows the radial profile of the coaxial jet velocity. Close to the nozzle exit, the difference in velocity between the outer jet and the inner jet is very distinct. This is captured by the computed result. As the coaxial jet evolves downstream, the inner and outer jet merge to form a smooth profile. Figure 6b compares the measured and calculated radial profiles of the axial velocity of the Mach 0.9 jet at 10% forward flight speed.

Figure 7 provides comparisons between measurements and predictions for two supersonic jets at Mach 1.37 and 1.67 at 10% forward flight velocity. The experimental data are taken from Refs. 21

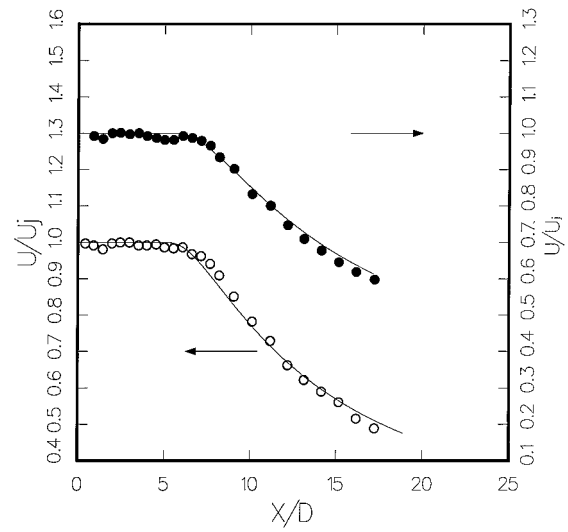

Fig. 3 Comparison between computed and measured centerline velocity distributions of a Mach 0.47 cold jet; experiment (Ref. 21): ○, $U_f/U_j = 0.1$; ●, $U_f/U_j = 0.2$; and ——, numerical result.

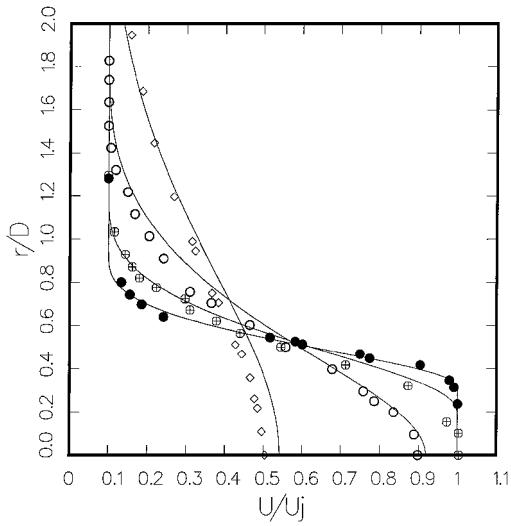

Fig. 4a Comparison between computed and measured axial velocity profiles of a Mach 0.47 cold jet at $U_f/U_j = 0.1$; experiment[21]: ●, $x/D = 1.63$; ⊕, $x/D = 3.25$; ○, $x/D = 7.50$; and ◇, $x/D = 16.0$; and ——, numerical result.

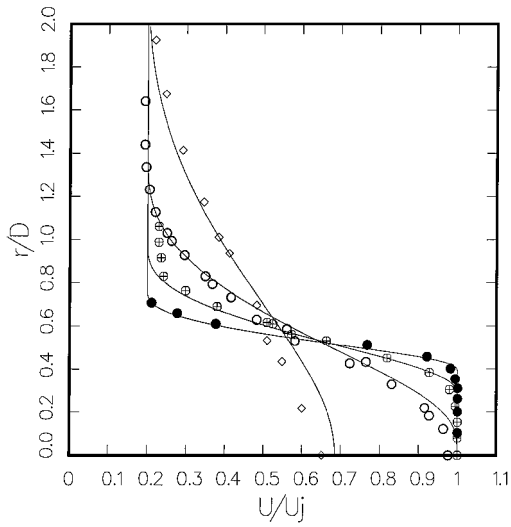

Fig. 4b Comparison between computed and measured axial velocity profiles of a Mach 0.47 cold jet at $U_f/U_j = 0.2$; experiment[21]: ●, $x/D = 1.63$; ⊕, $x/D = 3.5$; ○, $x/D = 7.0$; and ◇, $x/D = 16.0$; and ——, numerical result.

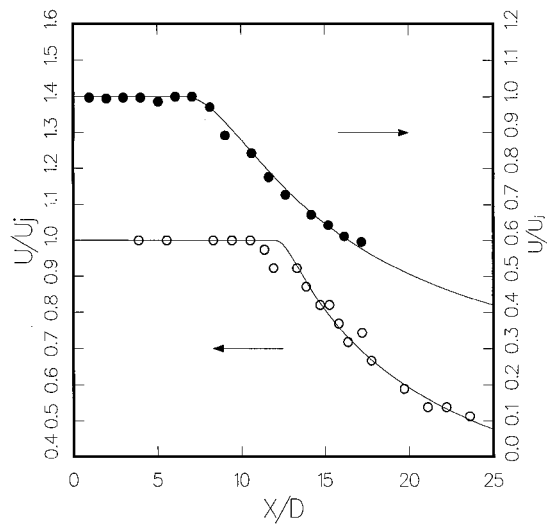

Fig. 5 Comparison between computed and measured centerline velocity distributions of a coaxial jet of Ref. 22 and a Mach 0.9 cold jet of Refs. 21 and 23 at $U_f/U_j = 0.1$; experimental data: ○, Ref. 22; ●, Refs. 21 and 23; and ——, numerical result.

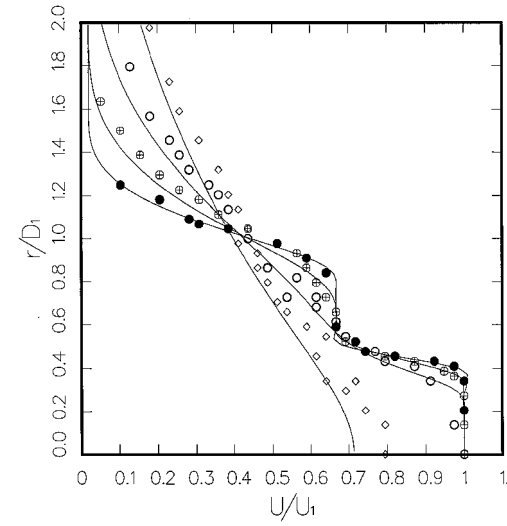

Fig. 6a Comparison between computed and measured axial velocity profiles of a coaxial jet with $U_1 = 411$ m/s, $T_1 = 657$ K, $D_1 = 3.92$ cm, $U_2 = 274$ m/s, $T_2 = 292$ K, $D_2 = 7.82$ cm; experiment[22]: ●, $x/D_1 = 2.0$; ⊕, $x/D_1 = 4.0$; ○, $x/D_1 = 8.0$; and ◇, $x/D_1 = 16.0$; and ——, numerical result.

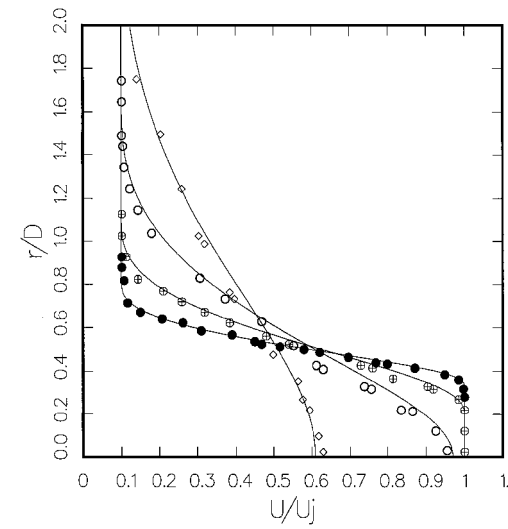

Fig. 6b Comparison between computed and measured axial velocity profiles of a Mach 0.9 cold jet at $U_f/U_j = 0.1$; experiment[21]: ●, $x/D = 2.0$; ⊕, $x/D = 4.0$; ○, $x/D = 8.0$; and ◇, $x/D = 16.0$; and ——, numerical result.

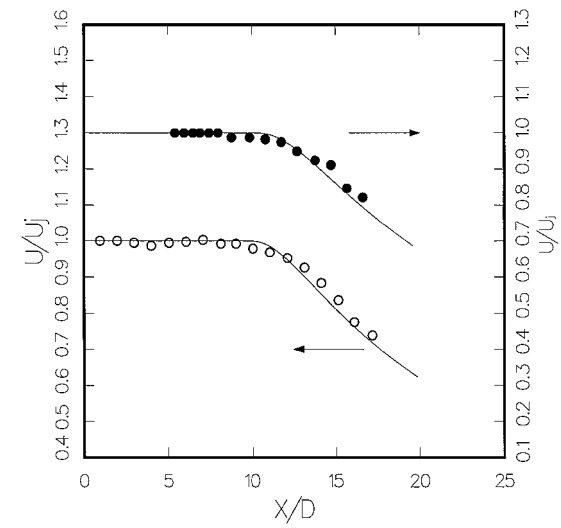

Fig. 7 Comparison between computed and measured centerline velocity distributions at $U_f/U_j = 0.1$; experiment[21,23]: ○, Mach 1.37 and ●, Mach 1.67 cold jet; and ——, numerical result.

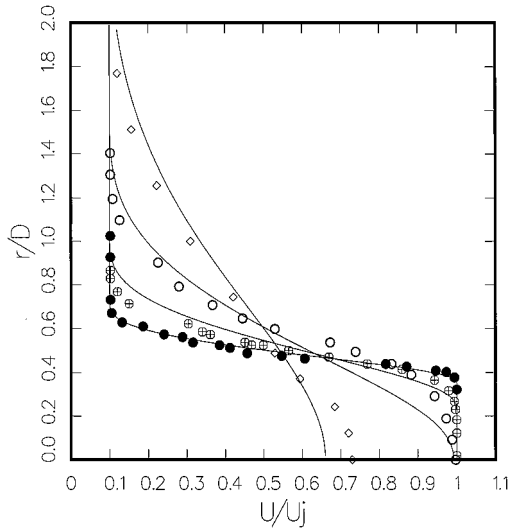

Fig. 8a Comparison between computed and measured axial velocity profiles of a Mach 1.37 cold jet at $U_f/U_j = 0.1$; experiment[21]: ●, $x/D = 2.0$; ⊕, $x/D = 4.0$; ○, $x/D = 8.0$; and ◇, $x/D = 16.0$; and ——, numerical result.

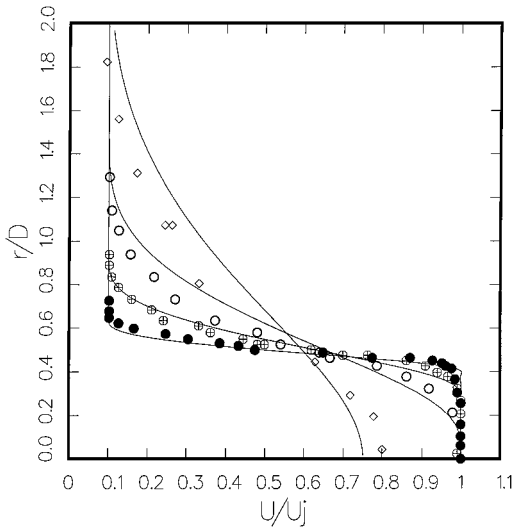

Fig. 8b Comparison between computed and measured axial velocity profiles of a Mach 1.67 cold jet at $U_f/U_j = 0.1$; experiment[21]: ●, $x/D = 2.0$; ⊕, $x/D = 4.0$; ○, $x/D = 8.0$; and ◇, $x/D = 16.0$; and ——, numerical result.

and 23. Figure 8a shows the radial distributions of the axial velocity of the Mach 1.37 jet. Figure 8b shows the corresponding velocity profiles for the Mach 1.67 jet.

Finally, Fig. 9 shows the measured velocity distributions of a hot coaxial jet with an inverted velocity profile from Ref. 24. Shown also are the computed velocity profiles. The inverted velocity profile, very prominent near the nozzle exit, diminishes in the downstream direction. At sufficiently far downstream, the merged jet exhibits a profile indistinguishable from that of a regular jet. In all of the preceding comparisons, there is good agreement in each case.

C. Comparison Between Calculated Far-Field Noise Spectra and Measurements

Once the mean flow velocity as well as the k and ε turbulence quantities are computed, the next step in the Tam and Auriault[17] theory is to calculate the adjoint Green's function according to Ref. 18. To find the far-field noise spectrum, all of these quantities are substituted into Eqs. (1) and (2). On performing the volume integration over the noise source region, the radiated noise spectrum in the far field is obtained.

Figure 10 shows the calculated and measured noise spectra of a Mach 1.5 jet from a convergent–divergent nozzle operating at design condition at three simulated forward flight Mach numbers. The data

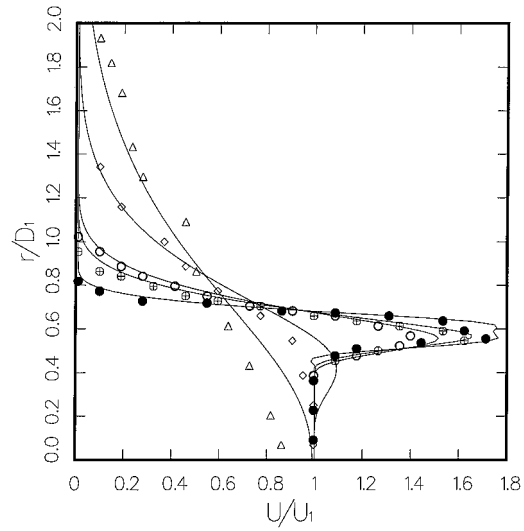

Fig. 9 Comparison between computed and measured axial velocity profiles of an inverted profile coaxial jet at $U_1 = 273$ m/s, $T_1 = 434$ K, $D_1 = 5.22$ cm, $U_2 = 477$ m/s, $T_2 = 758$ K, $D_2 = 7.14$ cm; experiment[24]: ●, $x/D_1 = 0.19$; ⊕, $x/D_1 = 1.35$; ○, $x/D_1 = 1.90$; ◇, $x/D_1 = 5.75$; and △, $x/D_1 = 11.5$; and ——, numerical result.

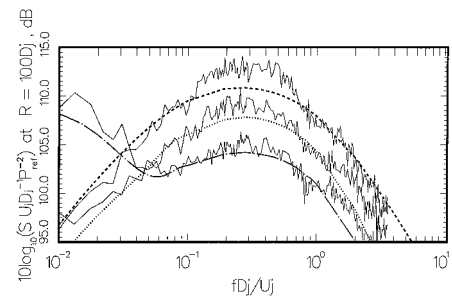

Fig. 10a Comparisons between measured and computed far field noise spectra of a Mach 1.5 cold jet at Θ = 60 deg: ——, experimental data[4]; and computed results: - - - -, $M_f = 0.0$; · · · ·, $M_f = 0.2$; and – · –, $M_f = 0.4$.

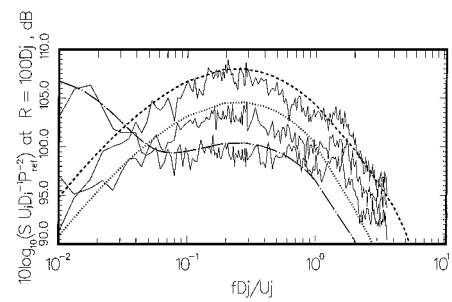

Fig. 10b Comparisons between measured and computed far field noise spectra of a Mach 1.5 cold jet at Θ = 90 deg: ——, experimental data[4]; and computed results: - - - -, $M_f = 0.0$; · · · ·, $M_f = 0.2$; and – · –, $M_f = 0.4$.

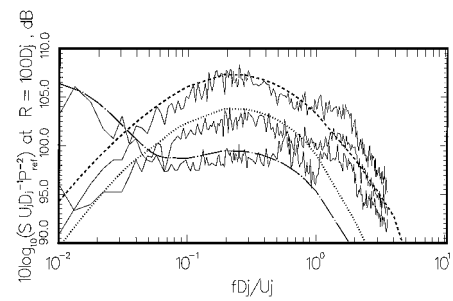

Fig. 10c Comparisons between measured and computed far field noise spectra of a Mach 1.5 cold jet at Θ = 100 deg: ——, experimental data[4]; and computed results: - - - -, $M_f = 0.0$; · · · ·, $M_f = 0.2$; and – · –, $M_f = 0.4$.

are from the work of Norum and Brown.[4] Figure 10a shows the spectra at $\Theta = 60$ deg measured from the jet exhaust direction. The top curve is for zero flight Mach number. The second curve is for flight Mach number 0.2. The bottom curve is for flight Mach number 0.4. It is easily seen that the calculated spectra are in good agreement with measurements. For each 0.2 increase in flight Mach number, there is approximately a 4.5-dB decrease in the measured peak noise level. This drop in the measured noise level is matched well by the computed results. At simulated forward flight Mach number 0.4, the jet noise is greatly reduced. This exposes the low-frequency mixing noise from the open wind tunnel. In Fig. 10a, the wind-tunnel noise is responsible for the low-frequency hump of the noise spectrum. This hump is predicted quite accurately by the theory.

Figures 10b and 10c show similar comparisons at $\Theta = 90$ and 100 deg, respectively. Again, there is good overall agreement between the measured and calculated spectra at simulated forward flight Mach numbers of 0.0, 0.2, and 0.4. When the measured spectra are examined carefully, it appears that they might have been slightly contaminated by high-frequency broadband shock associated noise. This may explain why the agreement at high frequencies is not as good.

Figure 11 shows the measured and calculated jet noise spectra for subsonic jets at various jet and flight Mach numbers, M_j and M_f. The data are from Ref. 21. Figure 11a is for spectra measured at $\Theta = 90$ deg. The jets are at Mach numbers 0.98, 0.73, and 0.51. For the particular facility used in the experiment, the open wind tunnel has to be turned on all of the time to avoid certain kinds of resonance. The static condition is represented by the case with a very small forward flight Mach number. The noise measurements in Ref. 21 are reported in one-third octave band. The data are converted to narrowband before being plotted in Fig. 11a. It is clear from Fig. 11a that the predictions match the measurements quite well for all Mach numbers. At subsonic jet Mach number, it appears that there is a 5 dB decrease in the noise spectrum for a 0.2 increase in forward flight Mach number. This reduction is reproduced well by the theory.

Figure 11b shows the corresponding change in the noise spectra at $\Theta = 60$ deg. Because of noise source convection and mean flow refraction effects, the spectra at $\Theta = 60$ deg are consistently 2–3 dB higher than those at $\Theta = 90$ deg. On considering that the theoretical predictions are tantamount to absolute predictions, it is deemed that there are good agreements between measurements and theory near the peak regions of the spectra. At high frequencies, the agreements are fair. It is not clear that the discrepancies here are due to contamination of the measured data (including the error involved in converting one-third octave band data to narrowband) or a deficiency of the theory. However, the Δ decibel changes between different flight Mach numbers appear to be quite accurately predicted.

III. Effects of Forward Flight on Jet Noise Source Distribution

The effects of forward flight on the mean flow of a high-speed jet are relatively well known. Obviously the presence of an outside flow reduces the shear gradient across the mixing layer of the jet. This then leads to a reduction in the jet spreading rate. With a smaller spreading rate, the potential core of the jet is lengthened.

The changes in the mean flow due to forward flight, in turn, alter the turbulence and the source of noise in the jet. In this section, we will investigate quantitatively the effects of forward flight on the noise source distribution by means of Eq. (2). Equation (2) provides the formula by which the far-field noise spectrum of a jet can be calculated. It has the form of a volume integral over the source location $\boldsymbol{x}_2$. A simple interpretation of this formula suggests that the integrand is the noise source. In the notation of the formula, the source is located at $\boldsymbol{x}_2$ and is responsible for radiating sound to the far-field observation point at $\boldsymbol{x}$ at frequency f ($\omega = 2\pi f$ is the angular frequency). Equation (2) contains the effects of mean flow refraction. Here our interest is on the source modification effects due to forward flight alone. For this purpose, we will restrict the observation point to $\Theta = 90$ deg. At this angle of radiation, the mean flow refraction effects are minimal.

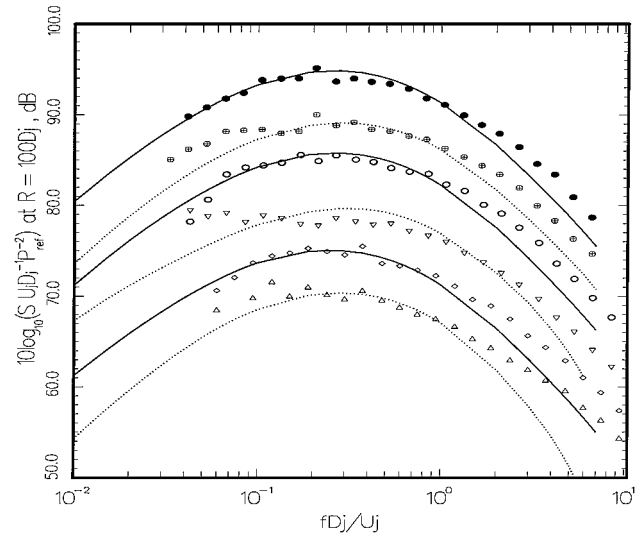

Fig. 11a Comparisons between measured and computed data for cold jets at $\Theta = 90$ deg; experiment[21]: ●, $M_j = 0.98$ and $M_f = 0.05$; ⊕, $M_j = 0.98$ and $M_f = 0.20$; ○, $M_j = 0.73$ and $M_f = 0.04$; ▽, $M_j = 0.74$ and $M_f = 0.20$; ◇, $M_j = 0.51$ and $M_f = 0.02$; △, $M_j = 0.51$ and $M_f = 0.10$; computed results, · · · · and ——.

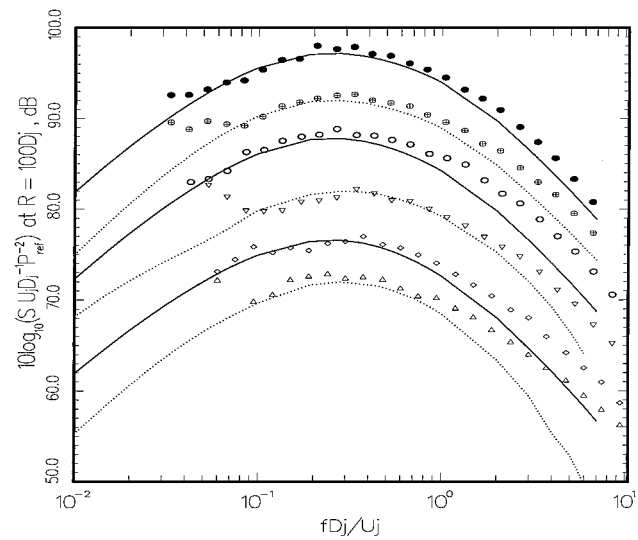

Fig. 11b Comparisons between measured and computed data for cold jets at $\Theta = 60$ deg; experiment (Ref. 21): ●, $M_j = 0.98$ and $M_f = 0.05$; ⊕, $M_j = 0.98$ and $M_f = 0.20$; ○, $M_j = 0.73$ and $M_f = 0.04$, ▽, $M_j = 0.74$ and $M_f = 0.20$, ◇, $M_j = 0.51$, and $M_f = 0.02$; △, $M_j = 0.51$, and $M_f = 0.10$; computed results, · · · · and ——.

When the preceding interpretation of Eq. (2) is followed, the formula for the axial distribution of noise sources for a slice of the jet between x_2 and $x_2 + \mathrm{d}x_2$ is $S_x(\boldsymbol{x}, x_2, \omega)\,\mathrm{d}x_2$, where

$$S_x(\boldsymbol{x}, x_2, \omega) = 4\pi \left(\frac{\pi}{\ell n 2}\right)^{\frac{3}{2}} \int_0^{2\pi}\int_0^{\infty} \frac{\hat{q}_S^2 \ell_S^3}{c^2 \tau_S} \times \left(\frac{|p_a(\boldsymbol{x}_2, \boldsymbol{x}, \omega)|^2 \exp\left[-\omega^2 \ell_S^2 \big/ \bar{u}^2 (4\,\ell n 2)\right]}{\left\{1 + \omega^2 \tau_S^2 [1 - (\bar{u}/a_\infty)\cos\Theta]^2\right\}} \right) r_2\,\mathrm{d}r_2\,\mathrm{d}\phi_2 \tag{8}$$

$$\mathrm{SPL}_x\left(\boldsymbol{x}, x_2, \frac{f D_j}{u_j}\right) = 10 \log\left[\frac{4\pi S_x(\boldsymbol{x}, x_2, \omega)}{\left(p_{\mathrm{ref}}^2 \big/ u_j\right)}\right] \tag{9}$$

where $\boldsymbol{x} = (R, \pi/2, \phi)$ is the observation point and $\boldsymbol{x}_2 = (r_2, \phi_2, x_2)$ is the source point. Sound pressure level (SPL_x) has the dimension of decibel per Strouhal number per unit axial length of the jet.

Another formula that is of interest to us is the azimuthally integrated noise source distribution, S_ϕ. This is the noise source

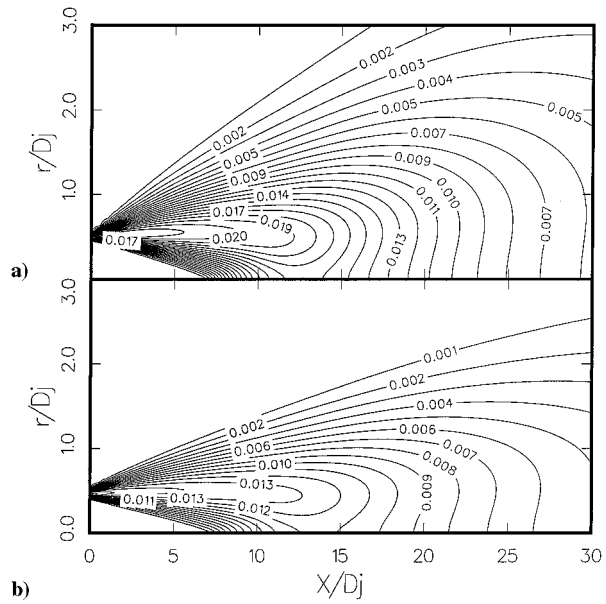

Fig. 12 Contours of k/u_j^2 in the x–r plane for a Mach 1.5 cold jet: a) $M_f = 0.0$ and b) $M_f = 0.3$.

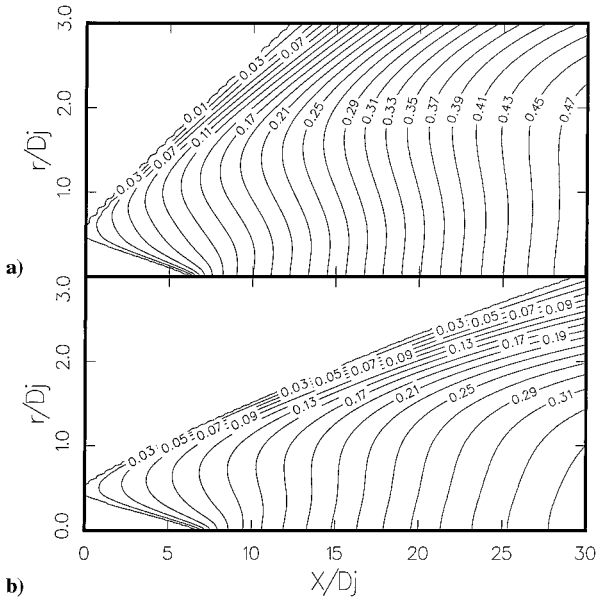

Fig. 13 Contours of l_s/D_j in the x–r plane for a Mach 1.5 cold jet: a) $M_f = 0.0$ and b) $M_f = 0.3$.

distribution in the x_2-r_2 plane with ϕ_2 integrated over from 0 to 2π. When starting from Eq. (2), the following expression for S_ϕ can easily be found:

$$S_\phi(\boldsymbol{x}, x_2, r_2, \omega) = 4\pi\left(\frac{\pi}{\ell n 2}\right)^{\frac{3}{2}} \int_0^{2\pi} \frac{\hat{q}_S^2 \ell_S^3}{c^2 \tau_S} \times \left(\frac{|p_a(\boldsymbol{x}_2, \boldsymbol{x}, \omega)|^2 \exp\left[-\omega^2 \ell_S^2 \big/ \bar{u}^2 (4\,\ell n 2)\right]}{\left\{1 + \omega^2 \tau_S^2 [1 - (\bar{u}/a_\infty)\cos\Theta]^2\right\}}\right) \mathrm{d}\phi_2 \tag{10}$$

$$\mathrm{SPL}_\phi = 10 \log\left[\frac{4\pi S_\phi D_j^2}{\left(p_{\mathrm{ref}}^2 \big/ u_j\right)}\right] \tag{11}$$

S_ϕ provides a measure of the radial distribution of the noise sources in a jet where the radial distance is measured in units of D_j.

A. Effects on Turbulence

Because the change in noise sources due to forward flight is a direct consequence of the change in jet turbulence, we will first examine the changes in turbulence intensity, the size of eddies responsible for noise radiation, and the eddy decay time. Figure 12a shows a contour map of the turbulence intensity (nondimensionalized by the square of the jet velocity), k/u_j^2, in the x_2-r_2 plane for a Mach 1.5 cold jet in static condition. For convenience, we will drop the subscript 2 and label the plane as the x–r plane so no confusion should arise. It is clear that the intensity is highest in the initial jet mixing layer. The intensity decreases in the downstream direction. Figure 12b shows the contour map for the same jet at 0.3 forward flight Mach number. When compared with Fig. 12a it is evident that forward flight at $M_f = 0.3$ reduces the turbulence intensity greatly. Also because the jet spreading is decreased, the jet turbulence is confined to a thinner mixing layer.

Figure 13a shows the contours of ℓ_S/D_j in the x–r plane for the Mach 1.5 cold jet in static condition, where ℓ_S is the typical size of noise producing eddies. Along the lip line where k is most intense, it is easy to see in Fig. 13a that ℓ_S increases almost linearly with downstream distance. The increase in eddy size in the downstream direction is expected on physical grounds. The linear increase is an indication of the self-similarity property of jet flows. Figure 13b shows the contours for the same jet at Mach 0.3 forward flight. A simple comparison of Figs. 13a and 13b indicates that the eddy size at the same location downstream is smaller with forward flight. The rate of increase in eddy size is also reduced. If one associates higher frequency sound to smaller eddies, then one expects an increase in high-frequency sound and simultaneously a decrease in low-frequency noise resulting in a slight shift of the noise spectrum to higher frequency. This is consistent with experimental measurements.

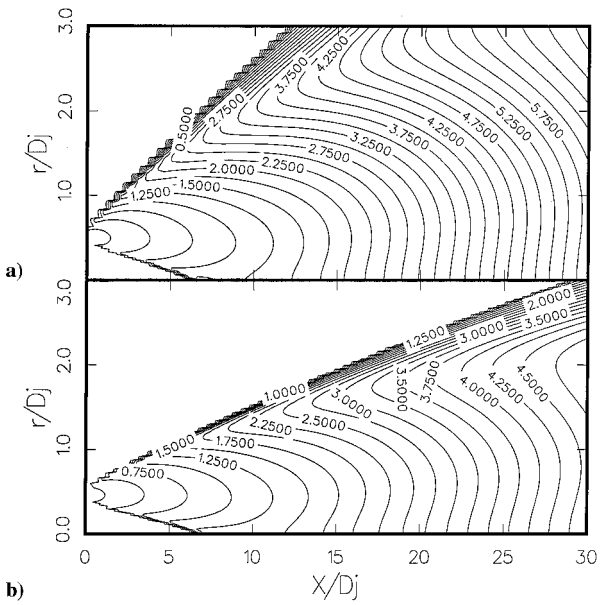

Fig. 14 Contours of $\tau_s u_j/D_j$ in the x–r plane for a Mach 1.5 cold jet: a) $M_f = 0.0$ and b) $M_f = 0.3$.

Figure 14a is a contour map of $\tau_S u_j/D_j$, the eddy decay time for the Mach 1.5 jet in a static condition. The eddy decay time increases in the downstream direction. Physically, it means that small eddies in the initial mixing layer of the jet decay much faster than the large eddies in the developed region of the jet. Figure 14b shows the contours at 0.3 forward flight Mach number. When the contours along the lip line of the jet are compared, it is clear that, up to 20 jet diameters downstream, the decay time is nearly unchanged by forward flight. This is somewhat unexpected.

We note that, although Figs. 12–14 show only the effects of forward flight on the turbulence characteristics of a Mach 1.5 jet, the trends are the same for jets at other Mach numbers, including subsonic jets. Qualitatively, one may use the relative changes indicated in Figs. 12–14 to estimate the corresponding changes for jets at other operating conditions.

B. Effects on Jet Noise Source Distribution

It is our intention to separate the effects of forward flight on the sources of jet noise from mean flow refraction effect. Therefore, in

presenting the noise source distribution we will fix the observer's coordinates to be at $R = 100D_j$ and $\Theta = 90$ deg as before. The mean flow refraction effects is minimal at 90-deg radiation. We will again drop the subscript 2 of the noise source coordinates of Eqs. (8–11), so no confusion should arise.

Figure 15a shows the calculated axial noise source distribution [see Eqs. (8) and (9)] of a Mach 1.5 cold jet in static condition for a number of Strouhal numbers, $Sr = f D_j/u_j$. Figure 15a indicates that the high-frequency noise sources are located very close to the nozzle exit. The low-frequency noise sources are located much farther downstream and extend well beyond the potential core of the jet. The noise source intensity peaks around Strouhal number 0.3. Spatially, the peak intensity is located near the end of the potential core. Figure 15b shows the distribution at 0.3 forward flight Mach number. It is evident from Figs. 15a and 15b that forward flight moves all of the noise sources downstream. The noise source intensity is significantly reduced for all frequencies.

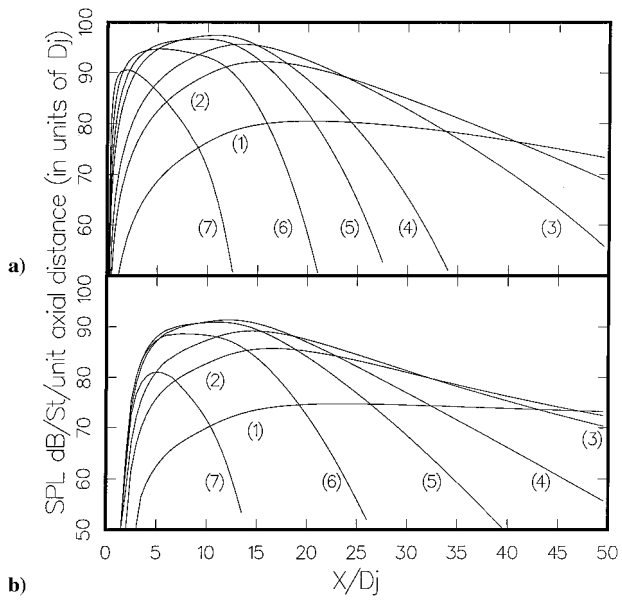

Fig. 15 Axial noise source distribution for an observer at $\Theta = 90$ deg and $R = 100D_j$, Mach 1.5 cold jet, 1) $Sr = 0.01$, 2) $Sr = 0.05$, 3) $Sr = 0.1$, 4) $Sr = 0.3$, 5) $Sr = 0.5$, 6) $Sr = 1.0$, and 7) $Sr = 3.0$: a) $M_f = 0.0$ and b) $M_f = 0.3$.

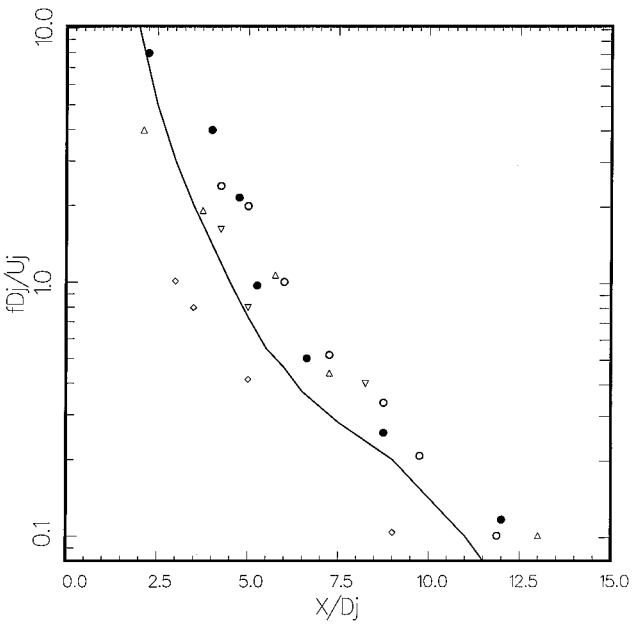

Fig. 16 Calculated and measured peak source strength locations; experiment, ●, acoustic mirror, $D = 20$ mm, $M_j = 1.0$; ▽, acoustic mirror, $D = 25$ mm, $M_j = 1.0$; ○, polar correlation, $D = 25$ mm, $M_j = 0.86$; △, polar correlation, $D = 51$ mm, $M_j = 0.86$ (Ref. 25); ◇, polar correlation, full-scale engine, 80% rpm (Ref. 26); and ——, model prediction, $M_j = 0.9$.

Figure 16 is a comparison of the measured and calculated peak source strength location as a function of Strouhal number for high subsonic jets. The experimental data are from Refs. 25 and 26. Experimentally, noise source location measurements are difficult to perform and are usually subjected to a high degree of uncertainty. Figure 16 shows good agreement between theory and experiment over a large range of Strouhal number (0.1–10). The good agreement lends confidence in the original jet noise theory of Ref. 17 from which Eqs. (8) and (9) are derived.

Figures 17–19 provide a measure of the changes in noise source distribution in the x–r plane due to forward flight. Figure 17 is for Strouhal number 0.01. It is representative of the low-frequency part of the spectrum. Figure 18 is for Strouhal number 0.3 (frequency at

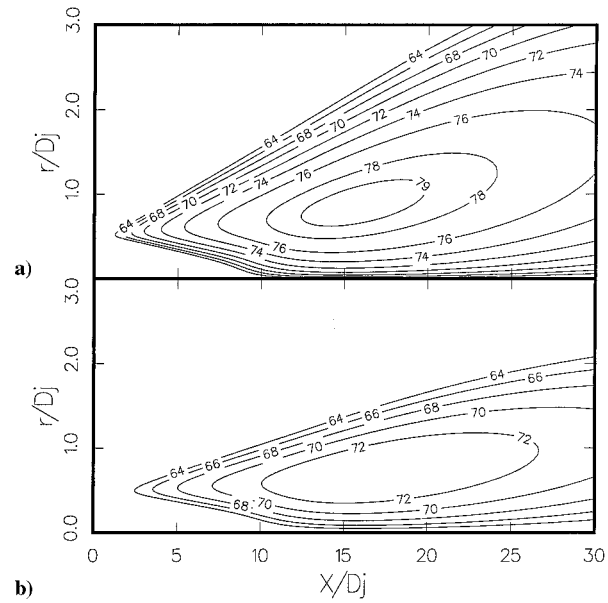

Fig. 17 Contours of azimuthally integrated noise source intensity in the x–r plane for an observer at $\Theta = 90$ deg and $R = 100D_j$, Mach 1.5 cold jet, $Sr = 0.01$, contours in units of SPL dB/Sr/unit area of x–r plane (length scale = D_j): a) $M_f = 0.0$ and b) $M_f = 0.3$.

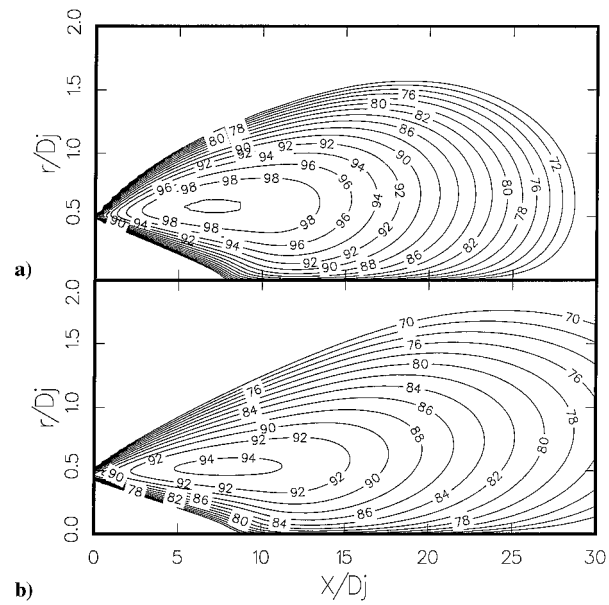

Fig. 18 Contours of azimuthally integrated noise source intensity in the x–r plane for an observer at $\Theta = 90$ deg and $R = 100D_j$, Mach 1.5 cold jet, $Sr = 0.3$, contours in units of SPL dB/Sr/unit area of x–r plane (length scale = D_j): a) $M_f = 0.0$ and b) $M_f = 0.3$.

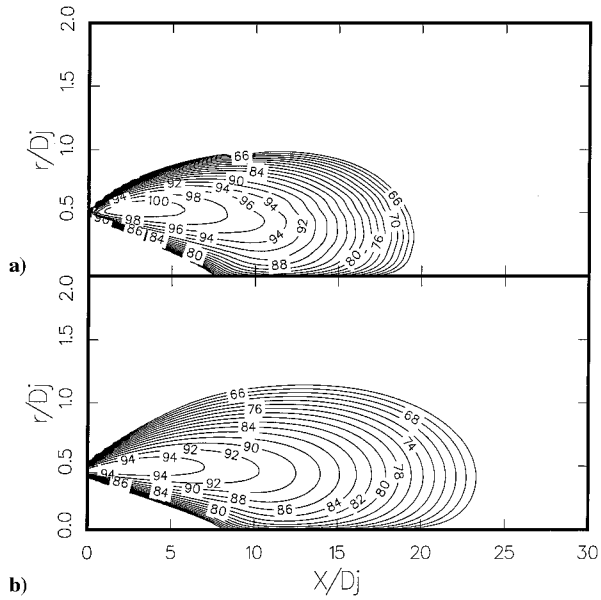

Fig. 19 Contours of azimuthally integrated noise source intensity in the x–r plane for an observer at $\Theta = 90$ deg and $R = 100D_j$, Mach 1.5 cold jet, $Sr = 1.0$, contours in units of SPL dB/Sr/unit area of x–r plane (length scale = D_j): a) $M_f = 0.0$ and b) $M_f = 0.3$.

maximum noise level). Figure 19 is for Strouhal number 1.0, representative of the high-frequency part of the spectrum. Figures 17–19 again indicate that the high-frequency noise sources are located close to the nozzle exit, whereas the low-frequency noise sources are located much farther downstream. The effect of forward flight is to move all of the noise sources downstream. In the radial direction the noise sources are most intense around the nozzle lip line, where the shear gradient of the mean velocity is largest. This is true even in forward flight. The sources are confined radially to the jet mixing layer both in the static condition and in flight.

One important point is that jet noise source distribution is not completely dependent on the turbulence intensity k distribution of the jet flow alone. This is clear by comparing Figs. 12 and 17. The obvious difference in the patterns of Figs. 12 and 17 indicates that the noise source is influenced not only by k but also by the eddy size and decay time of the eddies. The relationship is quite complex. It would be wrong to regard the noise of a jet is simply a function of k. Other aspects of jet turbulence are also important in the sound generation processes.

IV. Conclusions

In this paper, the effects of simulated forward flight on high-speed jet noise from fine-scale turbulence is investigated theoretically. The investigation is systematic, including the effects on the jet mean flow, the jet turbulence, the noise source distribution, as well as the far-field noise spectra in the sideline directions. Comparisons with experimental measurements are carried out in every step, limited only by the lack of data in the literature. Overall, very favorable agreements between theoretical predictions and experiments are found, suggesting that the basic theoretical framework is valid and that the model theory contains the essential physics of sound generation by turbulent shear flow.

The present study finds that forward flight can lead to significant reduction in jet turbulence intensity and noise source strength. This, in turn, leads to considerable reduction in the radiated noise. The reduction is nearly uniform across the entire frequency range of the spectrum. This is important in perceived noise level computation, which is used for aircraft certification.

From the point of view of noise suppression, knowledge of the location of the dominant sources of jet noise is important. The present investigation reveals that forward flight can move the noise sources over some distance downstream. Any development of a noise suppression device must take this into consideration if it is to remain effective at takeoffs and landings.

Acknowledgments

This work was supported by NASA Grant NAG 1-2145 and by Florida State University.

References

[1]Tanna, H. K., and Morris, P. J., "In-Flight Simulation Experiments on Turbulent Jet Mixing Noise," *Journal of Sound and Vibration*, Vol. 53, 1977, pp. 389–405.

[2]Larson, R. S., McColgan, C. J., and Packman, A. B.,"Jet Noise Source Modification Due to Forward Flight," *AIAA Journal*, Vol. 16, No. 3, 1978, pp. 225–232.

[3]Yu, J. C., and Dixson, N. R., "Experimental Study of Sound Radiation from Subsonic Jet in Simulated Motion," *AIAA Journal*, Vol. 18, No. 4, 1980, pp. 427–433.

[4]Norum, T. D., and Brown, M. C., "Simulated High Speed Flight Effects on Supersonic Jet Noise," AIAA Paper 93-4388, Oct. 1993.

[5]Cocking, B. J., "A Prediction Method for the Effects of Flight on Subsonic Jet Noise," *Journal of Sound and Vibration*, Vol. 53, 1977, pp. 435–453.

[6]Stone, J. R., "On the Use of Relative Velocity Exponents for Jet Engine Exhaust Noise," NASA TM 78873, 1978.

[7]Michalke, A., and Michel, U., "Relation Between Static and In-Flight Directivities of Jet Noise," *Journal of Sound and Vibration*, Vol. 63, 1979, pp. 602–605.

[8]Michalke, A., and Michel, U., "Prediction of Jet Noise in Flight from Static Tests," *Journal of Sound and Vibration*, Vol. 67, 1979, pp. 341–367.

[9]Tam, C. K. W., Golebiowski, M., and Seiner, J. M., "On the Two Components of Turbulent Mixing Noise from Supersonic Jets," AIAA Paper 96-1716, May 1996.

[10]Tam, C. K. W., "Jet Noise: Since 1952," *Theoretical and Computational Fluid Dynamics*, Vol. 10, 1998, pp. 393–405.

[11]Tam, C. K. W., and Burton, D. E., "Sound Generated by Instability Waves of Supersonic Flows. Part 1, Two-Dimensional Mixing Layer; Part 2, Axisymmetric Jets," *Journal of Fluid Mechanics*, Vol. 138, 1984, pp. 249–295.

[12]Tam, C. K. W., "Supersonic Jet Noise," *Annual Review of Fluid Mechanics*, Vol. 27, 1995, pp. 17–43.

[13]Tam, C. K. W., "Influence of Nozzle Geometry on the Noise of High-Speed Jets," *AIAA Journal*, Vol. 36, No. 8, 1998, pp. 1396–1400.

[14]Dahl, M. D., Papamoschou, D., and Hixon, R., "Supersonic Coaxial Jets: Noise Prediction and Measurements," AIAA Paper 98-2294, June 1998.

[15]Wat, J., Yamamoto, R., Golub, R., and Garber, D., "Comparison of Jet Mixing Noise Predictions with Data at High Subsonic Mach Number," AIAA Paper 99-1969, May 1999.

[16]Tam, C. K. W., and Zaman, K. B. M. Q., "Subsonic Jet Noise from Non-Axisymmetric and Tabbed Nozzles," *AIAA Journal*, Vol. 38, No. 4, 2000, pp. 592–599.

[17]Tam, C. K. W., and Auriault, L., "Jet Mixing Noise from Fine Scale Turbulence," *AIAA Journal*, Vol. 37, No. 2, 1999, pp. 145–153.

[18]Tam, C. K. W., and Auriault, L., "Mean Flow Refraction Effects on Sound Radiated from Localized Sources in a Jet," *Journal of Fluid Mechanics*, Vol. 370, 1998, pp. 149–174.

[19]Thies, A. T., and Tam, C. K. W., "Computation of Turbulent Axisymmetric and Nonaxisymmetric Jet Flows Using the k–ε Model," *AIAA Journal*, Vol. 34, No. 2, 1996, pp. 309–316.

[20]Tam, C. K. W., and Webb, J. C., "Dispersion-Relation-Preserving Finite Difference Schemes for Computational Acoustics," *Journal of Computational Physics*, Vol. 107, Aug. 1993, pp. 262–281.

[21]Plumblee, H. E., "Effects of Forward Velocity on Turbulent Jet Mixing Noise," NASA CR-2702, 1976.

[22]Lau, J. C., "A Study of the Structure of the Coannular Jet," Lockheed–Georgia Co., Rept. LG80 ER0017, Marietta, GA, 1980.

[23]Morris, P. J., "Turbulence Measurements in Subsonic and Supersonic Axisymmetric Jets in a Parallel Stream," *AIAA Journal*, Vol. 14, No. 10, 1976, pp. 1468–1475.

[24]Tanna, H. K., Tester, B. J., and Lau, J. C., "The Noise and Flow Characteristics of Inverted-Profile Coannular Jets," NASA CR-158995, 1979.

[25]Fisher, M. J., Harper-Bourne, M., and Glegg, S. A. L., "Jet Engine Noise Source Location: the Polar Correlation Technique," *Journal of Sound and Vibration*, Vol. 51, 1977, pp. 23–54.

[26]Tester, B. J., and Fisher, M. J., "Engine Noise Source Breakdown: Theory, Simulation and Results," AIAA Paper 81-2040, Oct. 1981.

P. J. Morris
Associate Editor